Journal of Coastal Research	15	1	168–185	Royal Palm Beach, Florida	Winter 1999

A Storm Surge Inundation Model for Coastal Planning and Impact Studies

Graeme D. Hubbert and Kathleen L. McInnes

Global Environmental Modelling Systems Warrandyte, Australia, 3113

CSIRO, Division of Atmospheric Research, Private Bag No. 1, Aspendale, Australia, 3195

ABSTRACT

HUBBERT, G. D. and MCINNES, K. L., 1999. A Storm Surge Inundation Model for Coastal Planning and Impact Studies. *Journal of Coastal Research*, 15(1), 168–185. Royal Palm Beach (Florida), ISSN 0749-0208.

A high resolution storm surge inundation model has been developed to model coastal flooding due to storm surges. The storm surge model, which features a nesting capability and inundation algorithm, is described. The flooding and draining rate is dependent on the modelled current in adjacent 'wet' grid cells which ensures realistic and smoothly varying results. Model simulations are carried out in two distinctly different geographic regions. The first of these is the town of Port Hedland on the northwest coast of Australia which was severely inundated by a tropical cyclone-induced storm surge in 1939. The model is shown to reproduce the peak flood levels and areas of inundation to a high degree of accuracy. Storm surge heights at the coast produced by a 'fixed-coastline' version of the model are compared with the inundation model results and indicate an overestimation of the storm surge heights by up to 17%. Simulations are conducted with varied horizontal resolution to investigate the robustness of the model. The flooding rates and areas of inundation are relatively unaffected by moderate variations in horizontal resolution. The second region studied is Port Phillip Bay, upon which the city of Melbourne is located. The model is used to simulate the storm surge and inundation produced by two separate cold fronts. The vulnerability of two locations within the Bay is investigated under altered sea level and storm strength conditions to demonstrate the potential impact of climate change. In a final simulation, levee banks on the tributaries draining into the bay are removed. The vastly increased inundation serves to illustrate the importance of maintaining and possibly increasing flood protection measures in this region in the future.

ADDITIONAL INDEX WORDS: *Tropical cyclones, cold fronts, coastal flooding, climate change, sea level rise.*

INTRODUCTION

Depth-integrated hydrodynamic models have wide application in the modelling of sea level heights and currents on continental shelves due to tidal forcing or storm surges. Applications of these models can include sea state and tidal forecasting, disaster planning and management, and coastal engineering and storm impact studies.

Hydrodynamic models can be sub-divided into two categories according to the method used in treating the coastal boundary that separates open water from land. In the first of these, referred to here as 'fixed-coast' models, the coastline is treated as an infinite wall against which water levels can rise and fall. This method is the simplest to implement, the most economical to run and suitable for model simulations requiring relatively low grid resolution (*i.e.* grid spacing of 1 km or greater) such as in operational storm surge forecasting. Examples of such applications can be found in HUBBERT *et al.* (1990, 1991), FLATHER *et al.* (1991), FLATHER (1994) and KONISHI (1995).

An alternative approach is to treat the land-water interface as a moving boundary with inland grid cells becoming flooded as sea levels at the coast increase due to rising tides or storm surges, and draining as the water recedes. For high resolution inundation forecasting (*e.g.* JARVINEN and LAWRENCE, 1985) or for flood level analysis, coastal planning and engineering applications where information on flood levels and inundation extent are required at relatively high horizontal resolution (i.e. grid spacings typically less than 1 km), this approach is the most suitable.

Increasing concern about anthropogenic climate change has created a greater awareness of the need to undertake impact studies in potentially vulnerable coastal regions. Storm surge inundation models are an ideal tool for addressing this problem. Important factors include the consequences of a mean sea level rise and possible changes to the frequency and intensity of severe storm surges. Storm surge inundation models can be used to investigate the implications of possible changes in terms of worst-case scenarios of flooding and can provide a basis for formulating mitigation strategies. For example, FLATHER and KHANDKER (1993) have undertaken a study to investigate the effects of a rise in sea level on storm surge inundation in the Bay of Bengal. The effects of sea level rise as well as changes in storm strength are also investigated in the present study for a location in southeastern Australia. In addition, the role of existing flood protection measures in the region are examined.

Various approaches for the treatment of moving boundaries in storm surge models can be found in the literature

97076 received and accepted in revision 20 April 1997.

and a review of these methods is given in FLATHER and HUBBERT (1990). The majority of models employ techniques whereby grid cells are incrementally added to or subtracted from the computational domain according to a set of prescribed conditions being satisfied. The usual assumptions are that the normal component of the velocity at the land-sea interface is assumed to be zero and grid cells are defined as having flooded or drained according to criteria based on the height of the water relative to the topographic height at adjacent land points. As shown by FALCONER and OWENS (1987), this method can produce noisy and even unstable results, particularly when grid resolution is reduced. However, they show that a more heavily constrained drying procedure can alleviate these problems. Other models which employ this approach are described in REID and BODINE (1968), LEENDERTSE and GRITTON (1971) and YEH and CHOU (1979). The method described in FLATHER and HEAPS (1975) is similar although the wetting and drying constraints also take into account the gradient of the water surface. REID and BODINE (1968) include empirical formula based on flow over weirs to determine flow rates at the coastal boundary when new grid cells become flooded. SIELECKI and WURTELE (1970), on the other hand, have developed a method to compute water level by linearly extrapolating water depths at the coastal boundary. Their technique is applied to idealised situations for which analytical solutions exist, rather than the more complex geometries which usually characterise coastal regions.

The model developed in the present study utilises a methodology for wetting and drying which depends not only of the sea surface height relative to the adjacent topography, but also to the distance travelled by the coastal interface based on the velocity of the current immediately seaward of the boundary. This means that the inclusion or removal of a grid-point may take more than a single time step to accomplish even though the height criterion may be satisfied. Instantaneous wetting and drying of grid cells, which can generate noise in the numerical solutions, is therefore minimised. This technique is found to be extremely robust in complex terrains, under severe atmospheric forcing conditions and a wide range of grid spacings.

The remainder of the paper is organised as follows. In Section 2, the storm surge model and inundation algorithm are described in detail. The performance of the model is demonstrated in Section 3 by simulating an intense tropical cyclone. Results are compared with simulations conducted with fixed-boundary conditions. The impact of changes in grid resolution are also explored. In Section 4, the model is used to simulate two mid-latitude cold fronts within a partly enclosed bay in southeastern Australia. Sensitivity experiments are conducted to explore the impact of increased sea levels and atmospheric storm strength on the storm surge heights and areas of inundation. The importance of existing levee banks on tributaries flowing into the bay are also demonstrated. Finally concluding comments are presented in Section 5.

THE MODEL

Equations

The non-linear, depth-integrated momentum equations and continuity equation solved by the model are:

$$\frac{\partial U}{\partial t} = fV - mg\frac{\partial \zeta}{\partial x} - \frac{m}{\rho_w}\frac{\partial P}{\partial x} - m\left(U\frac{\partial U}{\partial x} + V\frac{\partial U}{\partial y}\right) + \frac{1}{\rho_w H}(\tau_{sx} - \tau_{bx}) - \nu\nabla^2 U, \quad (1)$$

$$\frac{\partial V}{\partial t} = -fU - mg\frac{\partial \zeta}{\partial y} - \frac{m}{\rho_w}\frac{\partial P}{\partial y} - m\left(U\frac{\partial V}{\partial x} + V\frac{\partial V}{\partial y}\right) + \frac{1}{\rho_w H}(\tau_{sy} - \tau_{by}) - \nu\nabla^2 V, \quad (2)$$

$$\frac{\partial \zeta}{\partial t} = -m^2\left[\frac{\partial}{\partial x}\left(\frac{UH}{m}\right) + \frac{\partial}{\partial y}\left(\frac{VH}{m}\right)\right], \quad (3)$$

where U and V are the depth averaged currents in the x and y directions respectively, H is the total water depth, ζ is the sea surface elevation, f is the Coriolis parameter, g is the acceleration due to gravity, m is the map factor (a scaling factor dependent on the chosen map projection of the model grid), P is the atmospheric surface pressure, ρ_w is the water density, ν is the coefficient of viscosity and τ_{sx} and τ_{sy} represent the surface wind stress and τ_{bx} and τ_{by}, the bottom frictional stress in the x and y directions, respectively.

The surface wind stress components are computed using the quadratic relationship:

$$\tau_{sx} = C_D\rho_a|\mathbf{u}_a|u_a, \qquad \tau_{sy} = C_D\rho_a|\mathbf{u}_a|v_a, \quad (4)$$

where $|\mathbf{u}_a| = (u_a^2 + v_a^2)^{1/2}$, u_a and v_a are the horizontal components of wind velocity near the ocean surface, ρ_a is the density of air, and C_D is the drag coefficient based on SMITH and BANKE (1975) and expressed as follows:

$$C_D = \begin{cases} |0.63 + 0.066|\mathbf{u}_a|| \times 10^{-3}, & |\mathbf{u}_a| < 20 \text{ m s}^{-1}; \\ |2.28 + 0.033(|\mathbf{u}_a| - 20.0)| \times 10^{-3}, & |\mathbf{u}_a| > 20 \text{ m s}^{-1}. \end{cases} \quad (5)$$

The bottom stress is represented by a Manning's n depth-dependent friction relation following SIGNELL and BUTMAN, (1992):

$$\tau_{bx} = \rho_w\frac{gn^2}{(H + \zeta)^{1/3}}(U^2 + V^2)^{1/2}U, \qquad \tau_{by} = \rho_w\frac{gn^2}{(H + \zeta)^{1/3}}(U^2 + V^2)^{1/2}V, \quad (6)$$

where n has the value 0.0264. This formulation ensures that the drag coefficient increases with decreasing water depth and is applied to water depths greater than 1 m. In extremely shallow water and over land points that become inundated, drag coefficients are specified at each gridpoint according to the terrain type.

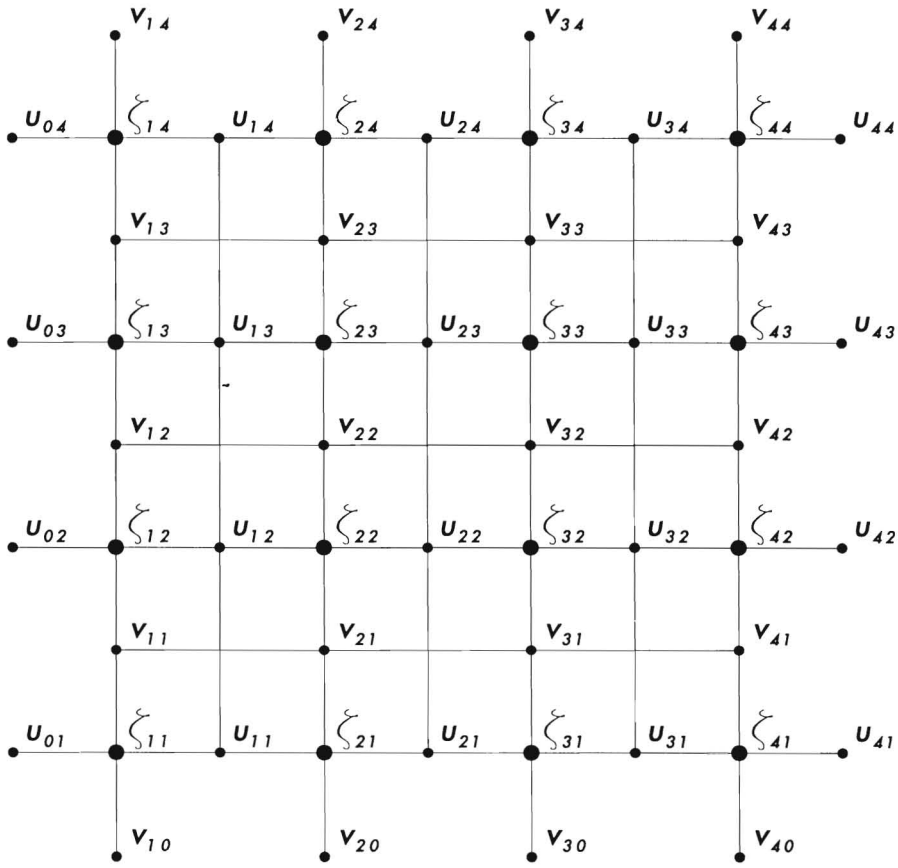

Figure 1. The Arakawa-C grid over which the model equations are solved.

Numerical Technique

Equations (1)–(3) are solved on an Arakawa C-grid (Figure 1) (MESINGER and ARAKAWA 1976, p. 47) using a split-explicit finite-difference scheme. Full details can be found in HUBBERT *et al.* (1990) although a brief description will be given here. The continuity equation and the gravity wave and Coriolis terms in the momentum equations are solved on the shortest time step, known as the *adjustment* step, using the forward-backward method. The non-linear advective terms are solved on an intermediate *advective* time step using the two-time-level method of MILLER and PEARCE (1974). Finally, on the longest time step, the so-called *physics* step, the surface wind stress, bottom friction stress and atmospheric pressure are solved using a backward-implicit method.

The storm surge model and all ancillary programs such as the grid generator, programs for generating atmospheric boundary conditions and various plotting programs have been coded in FORTRAN and run on Personal Computers (PCs) under the DOS operating system (or DOS running under Windows 3.1 or Windows 95).

Boundary Conditions

The storm surge model can be run in one of two ways. It can be run in isolation over a region of interest or a series of simulations can be performed over successively smaller and higher resolution grids centred on the region of interest using a technique called 'one-way nesting'. This approach is an economical way of maximizing the accuracy of the highest resolution simulation without needing to use a prohibitive number of gridpoints, since the lower resolution outer simulation provides the boundary conditions for the nested simulation. In the present study, single nesting is used which requires an outer and one nested simulation.

The low resolution model simulations are carried out over each of the two large domains indicated in Figure 2. On the open boundaries, the sea surface elevation is obtained from $\zeta^n = \zeta^{n*} + \Delta\zeta^T + \Delta\zeta^M$ where ζ^n is the height at the current time step, ζ^{n*} is a provisional value of ζ obtained by solving (3) on the grid configuration shown in Figure 1, $\Delta\zeta^T$ and $\Delta\zeta^M$ are the incremental changes in tidal height and atmospheric barometric displacement which have occurred since the previous time step. A radiation boundary condition, which solves for the group velocity, is used to compute the velocity components on outflow boundaries (MILLER and THORPE, 1981) while a zero-gradient condition is used on inflow boundaries. At the coastal boundary of the larger domain, the coastline is fixed and so the normal component of velocity is zero.

The nested simulations are conducted over the three smaller regions indicated in Figure 2. The low resolution simulated

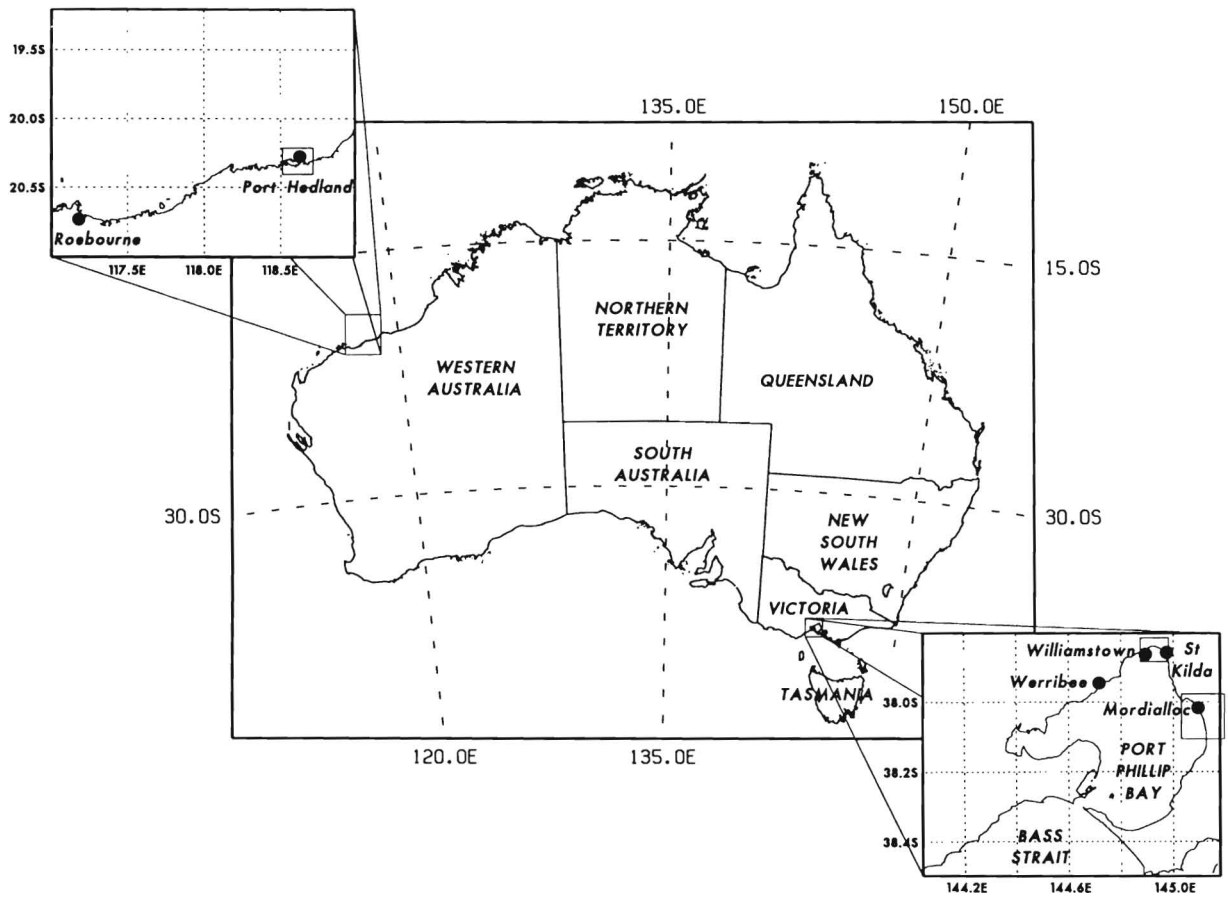

Figure 2. Map showing the location of the Port Hedland and Port Phillip Bay study regions. The two magnified maps show the areas over which the outer low resolution storm surge model simulations are performed. The rectangles within these maps, show the regions over which the high resolution inundation modelling is performed.

fields are interpolated to the high resolution grid and applied as boundary conditions using a weighted cosine function which smoothly blends model predicted values on the inner grid with those from the low resolution grid over a specified number of gridpoints in from the boundary. If tidal effects are not included in the low resolution simulation, then they also must be specified on the boundaries of the inner grid. On the coastal boundaries, equations (1)–(3) are solved assuming that the normal component of the velocity is zero. Following this calculation procedure, the inundation technique is then applied to determine whether the coastline requires repositioning.

Inundation Algorithm

The adjustment of coastlines to account for flooding and draining takes place after equations (1)–(3) have been solved as described above. The coastal boundary is configured to pass through the velocity gridpoints on the staggered grid in a stepwise manner such that it passes through the U points in the y-direction and through V points in the x-direction. The velocities on the boundaries are assumed to be zero.

The first step is to calculate the distance in the x- and y-directions that fluid could travel in a time step at each ζ gridpoint which is adjacent to the coast. The depth-averaged current velocity used in this calculation is taken at the first gridpoint on the seaward side of the ζ grid-point. The travel distance is:

$$\Delta X^n_{i,j} = \Delta X^{n-1}_{i,j} + \Delta t \times \begin{cases} U^n_{i-1,j}, & U > 0 \\ U^n_{i,j}, & U < 0 \end{cases} \tag{7}$$

$$\Delta Y^n_{i,j} = \Delta Y^{n-1}_{i,j} + \Delta t \times \begin{cases} V^n_{i-1,j}, & V > 0 \\ V^n_{i,j}, & V < 0 \end{cases} \tag{8}$$

where $\Delta X^{n-1}_{i,j}$ and $\Delta Y^{n-1}_{i,j}$ are the distances the water travelled in the previous time step. By factoring in the travel time of the fluid, inland grid cells are prevented from automatically becoming inundated at the first instant the water level at the coast exceeds the height of the adjacent dry points. In (7) and

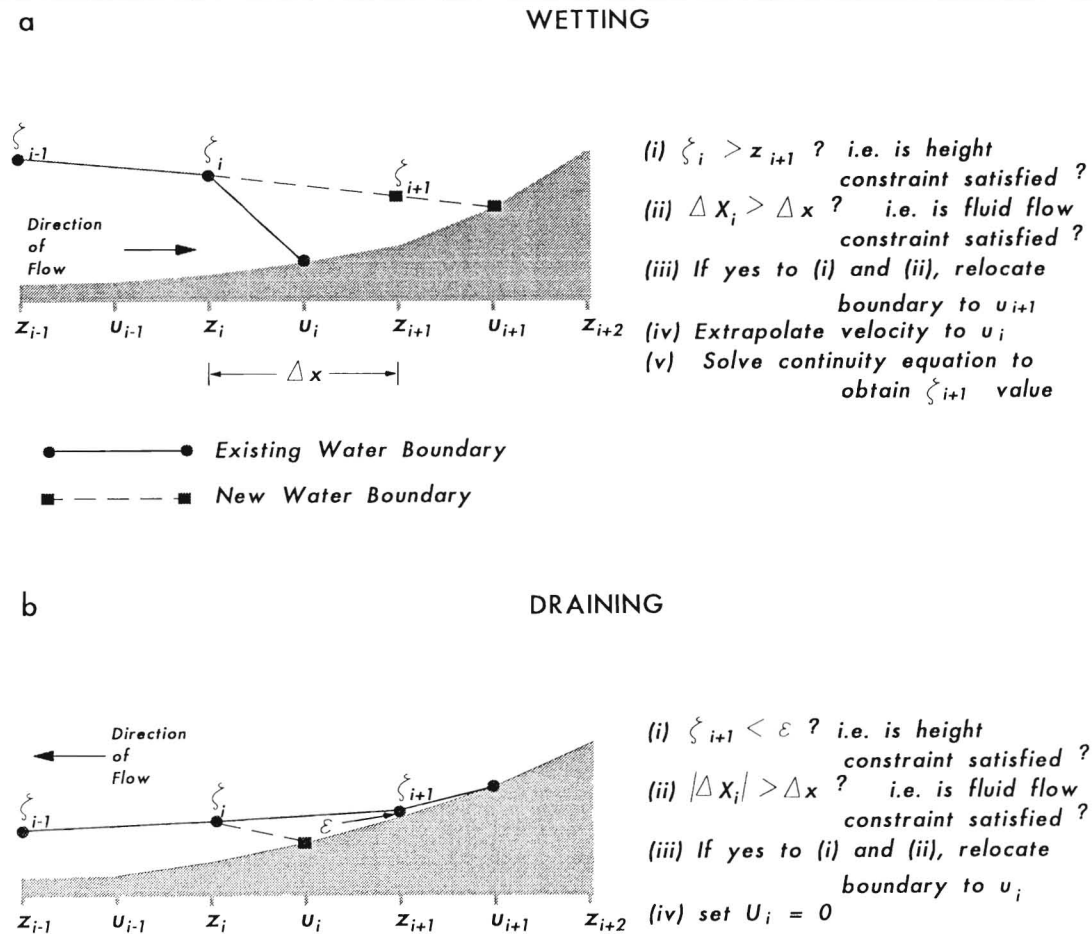

Figure 3. Schematic illustrating (a) the wetting and (b) the draining procedure in the inundation model. Note that the procedure is illustrated for the x-direction only and z and u on the horizontal axis are used to represent locations where the sea surface elevation ζ, and the depth-averaged current, U, are calculated.

(8), the first option applies to flooding in the positive x or y direction (or draining in the negative x and y direction) while the second option applies to flooding in the negative x and y direction (or draining in the positive x and y direction).

The testing for coastline movement proceeds in the x- and y-directions separately. If the height of the water at the first z-point seaward of the coastline exceeds the topographic height at the first z-point landward of it (Figure 3A), and the accumulated distance travelled in the given direction exceeds the grid separation, then a new sea-point is added to the computational domain. The velocity at the newly acquired velocity point is extrapolated from adjacent points and (3) is solved to obtain the water depth at the new height point. Finally, $\Delta X^n_{i,j}$ and $\Delta Y^n_{i,j}$ are re-set to zero.

The procedure for draining is similar. If the height of the fluid at the height point adjacent the boundary drops below some arbitrary positive height, ϵ, (Figure 3B) and the accumulated distance travelled by the fluid, exceeds the grid length, then draining is assumed to have occurred. The height gridpoint is reclassified as dry (i.e. $\zeta = 0$) and the boundary relocated to the adjacent wet velocity gridpoint.

APPLICATION TO TROPICAL CYCLONE INUNDATION

Background

In this section, the model performance is examined under the forcing provided by a severe tropical cyclone on Australia's northwest shelf. Whilst a number of tropical cyclones have passed near Port Hedland in recent years, most surges have not coincided with a rising tide, or the coastal crossing point has been to the east of the town, producing offshore winds and a negative surge. The most significant event to affect Port Hedland in recent history occurred on January 11, 1939. This cyclone produced maximum sustained winds in Port Hedland of around 130 km h^{-1} with gusts to 160 km h^{-1}. Approximately one third of the buildings in the town were destroyed, largely due to the wind waves and storm surge. Flood waters completely isolated the town for several hours producing peak flood levels of 5.7 m above mean sea level.

The historical significance of this cyclone event in Port Hedland has ensured that considerable information about the event, including aerial photography of the extent of the storm

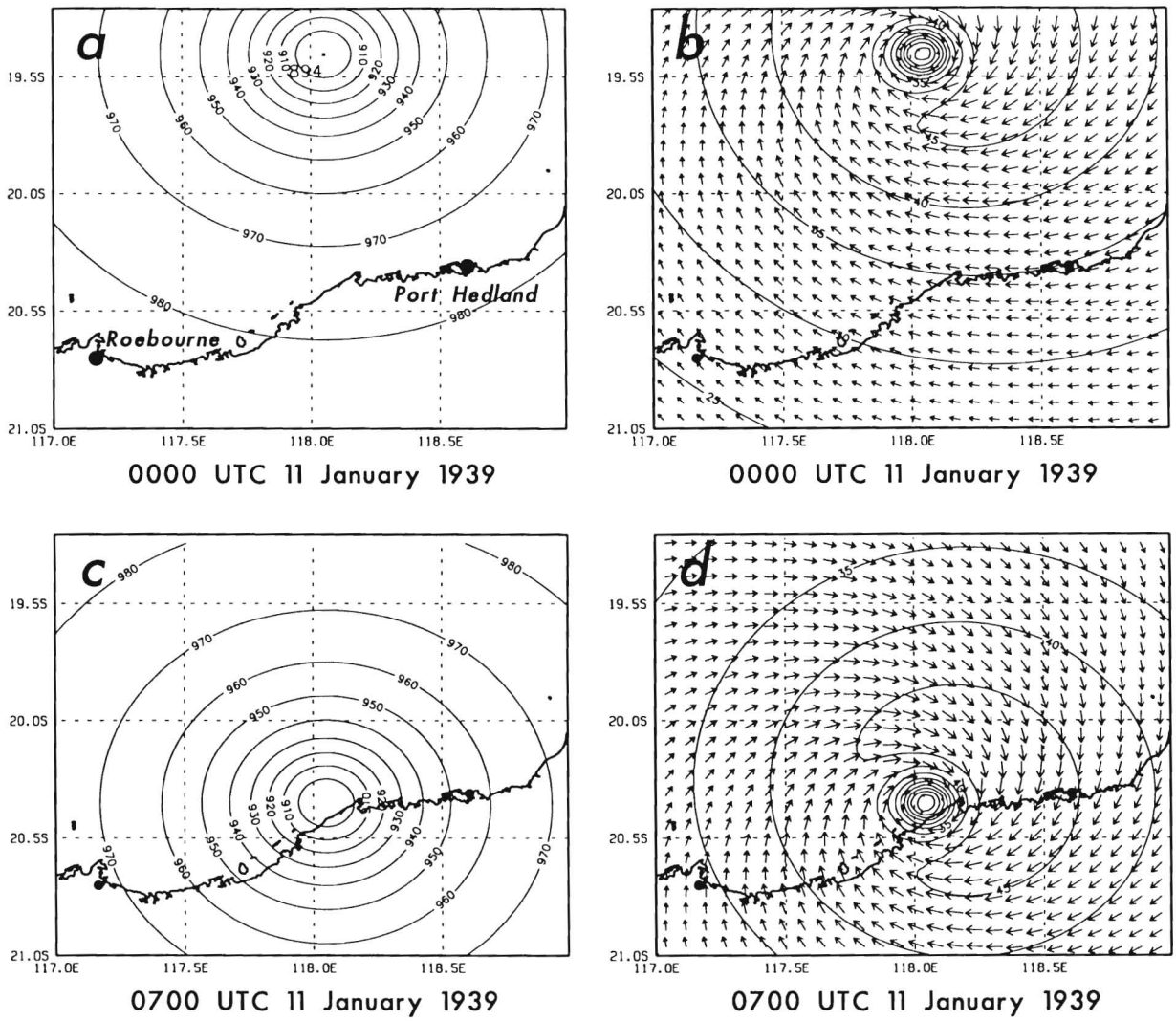

Figure 4. (a) Modelled cyclone pressure and (b) surface wind field as the cyclone approaches the coast from the north, and (c) pressure and (d) winds at the time of coastal crossing.

surge inundation are available for model verification. This event has therefore been chosen to demonstrate the storm surge inundation model.

Meteorological Input

The surface pressure and wind fields during the cyclone event, required to drive the storm surge model, were reconstructed by fitting an analytical tropical cyclone model based on HOLLAND (1980) as described in HUBBERT *et al.* (1991) to available meteorological observations in the region. The exact path and point of coastal crossing are not known however, estimates made at the time of storm passage, suggested it followed a southward trajectory for the duration of its influence on Port Hedland and made landfall 28 km west the town. The minimum pressure at Port Hedland was 954 hPa and occurred between 0630 and 0730 UTC 11 January. Roebourne, at that time, recorded a minimum of 972 hPa. The specification of central pressure and radius of maximum winds in the cyclone model was made so that the resulting winds and pressure best fit the observations. These fields were generated for the 48 hours from 0000 UTC January 11. The best fit was found with a central pressure of 895 hPa, a 30 km radius of maximum winds, a Holland B parameter of 1.0 and a coastal crossing point 60 km to the west of Port Hedland. It worth noting that this central pressure is 10 hPa lower than the minimum previously recorded for a cyclone in this region. The cyclone wind and pressure fields are shown in Figure 4.

The effects of rainfall have been ignored in the present study. Although considerable rainfall (in excess of 150 mm) and serious flooding were reported at various inland stations, the rapid onset of the storm surge at the coast suggests that

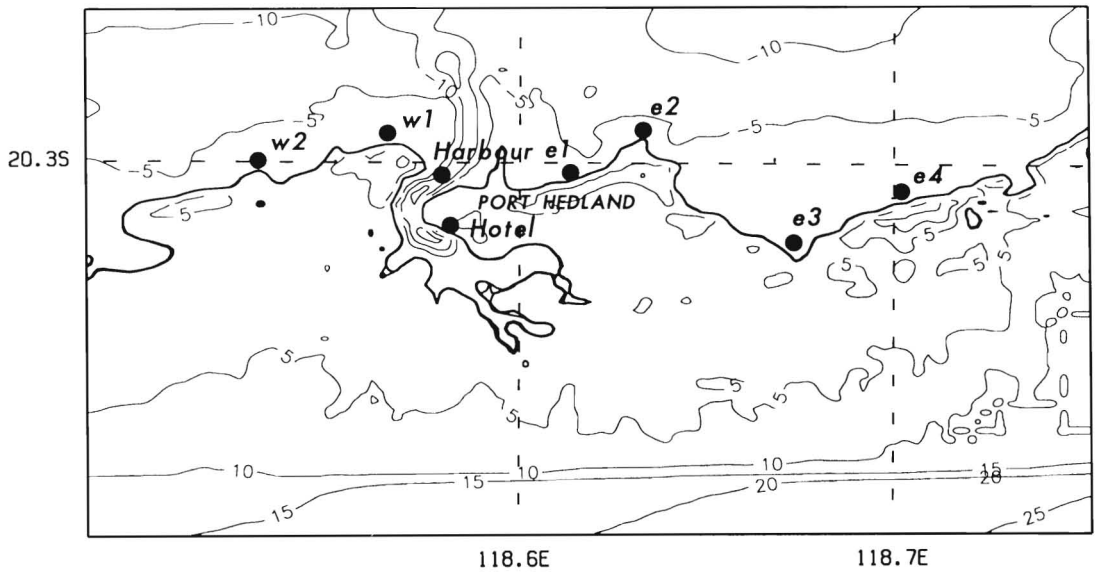

Figure 5. The fine mesh model domain showing topography and bathymetry at 5 m contours. Also shown are the coastal locations where storm surge heights are compared using the fixed boundary and moving boundary conditions. The hotel and township are also marked.

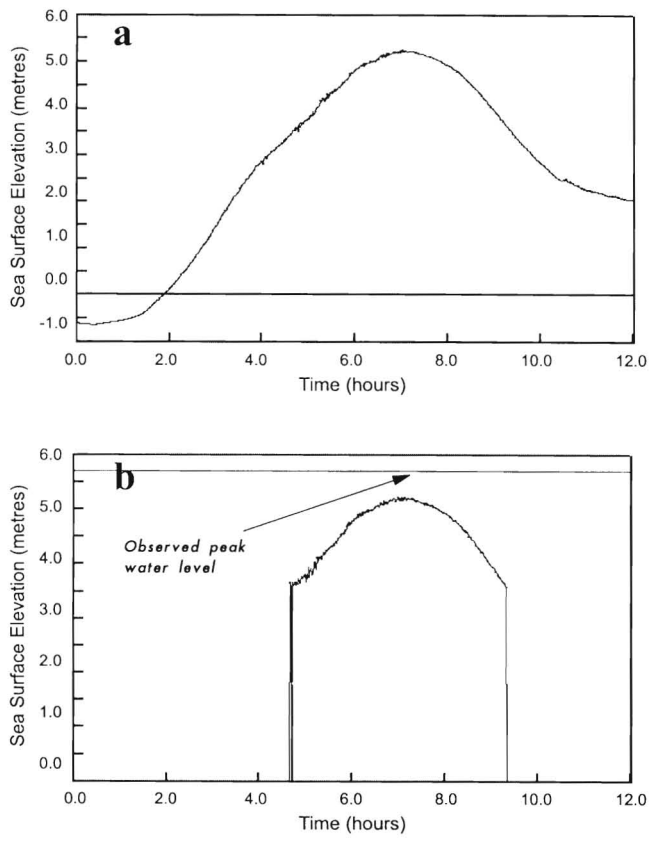

Figure 6. Time series showing the sea level height at (a) Port Hedland Harbour and (b) the hotel. The actual water level inside the hotel reached 5.7 m.

run-off was not likely to have made a significant contribution to water levels at the time of the storm surge peak.

Model Methodology

Model simulations of the storm surge were conducted on the lower resolution outer grid shown in Figure 2 at 1 km resolution. The model was then run over the fine resolution inner grid encompassed by Figure 5 at 150 m resolution with sea level heights from the outer model and tidal information applied on the open boundaries.

Bathymetry closely approximating the Port Hedland Harbour as it was in 1939 was recreated using old shipping charts and records for the simulation of the 1939 storm surge in section 2d. The major changes which have occurred in recent times are the dredging of the harbour and the creation of the spoil bank to the north of the township. It should be noted that the simulations discussed in sections 2e and 2f were conducted at a later stage and, for reasons of practicality, utilized the modern day topography and bathymetry which is shown in Figure 5.

Tides, Waves and Modelling Results

The high tide level at Port Hedland harbour on 11 January during the cyclone event was 2.08 m above mean sea level at 0639 UTC. The inundation model, when run with tidal forcing from the M_2, N_2, K_2, S2, K_1, and O_1 tidal constituents applied at the boundary of the inner grid, produced a high tide of 2.10 m at 0640 UTC at Port Hedland Harbour. The difference in water elevation of 0.02 m indicate close agreement between the modelled tides and predicted high tide at Port Hedland on that day.

Wave set-up and run-up for a range of storm surges and tidal heights at Port Hedland have been modelled by Lawson

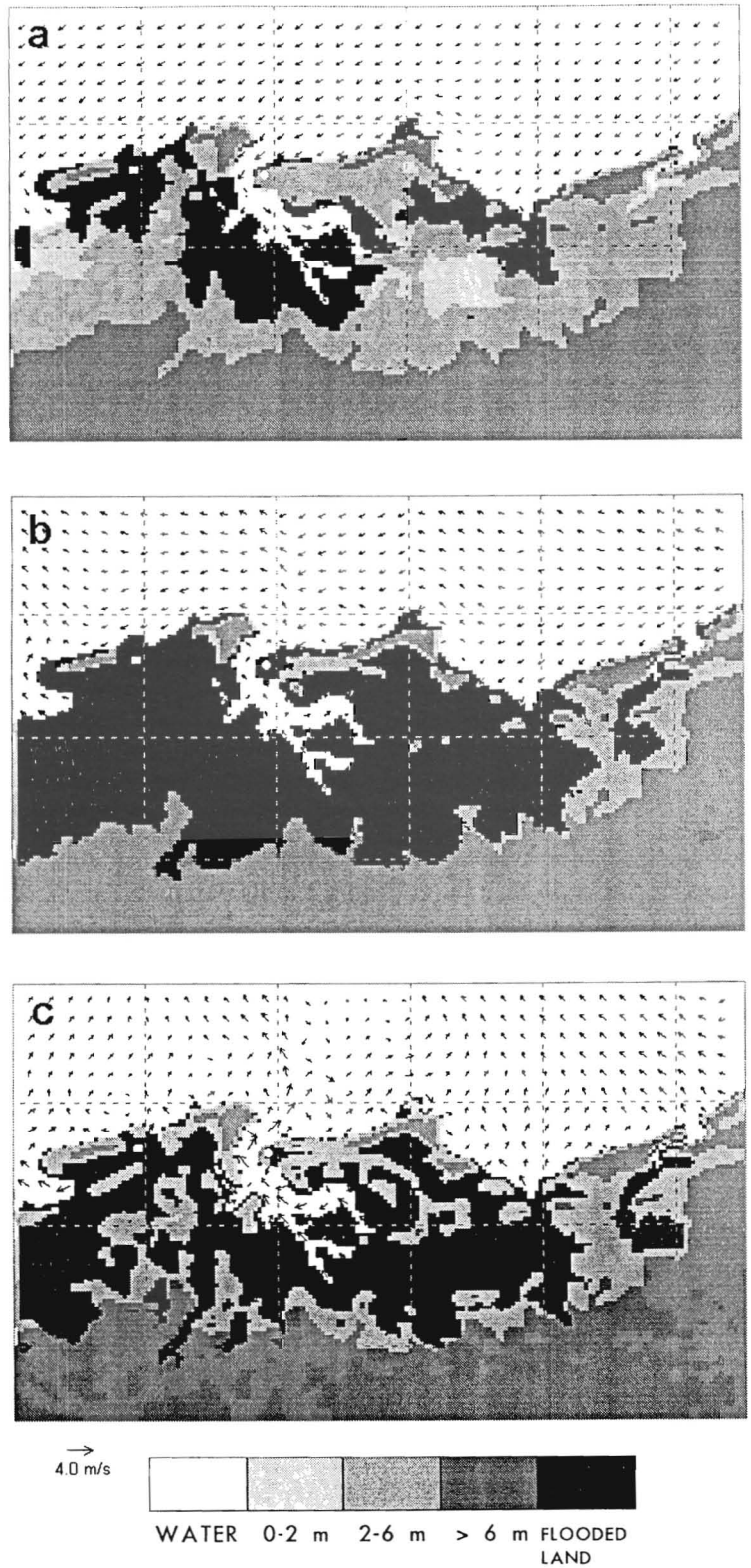

Figure 7. The storm surge inundation produced by the model at (a) 0500 UTC, (b) 0800 UTC and (c) 1100 UTC on 11 January 1939. Grid lines are shown every 5 km.

Table 1. *Summary of the inundated grid cells and the area this represents at the times indicated for model simulations conducted at 150, 225 and 300 m* resolution. The mean and standard deviation of the results are also tabulated.

Time (UTC)	150 m Gridpoints	150 m Area (km^2)	225 m Gridpoints	225 m Area (km^2)	300 m Gridpoints	300 m Area (km^2)	Mean (km^2)	Standard Deviation (%)
0500	1339	52	1170	58	472	51	54	10
0600	4936	111	2362	119	1283	115	115	5
0700	6217	140	3141	159	1677	151	150	9
0800	6687	150	3320	168	1814	163	160	8
0900	6182	139	3058	155	1655	149	148	8
1000	5400	121	1614	131	1435	129	127	6
1100	4936	111	2244	113	1195	107	110	4

and Treloar Pty Ltd using the Danish Hydraulics Institute wave model (SPECIAL SERVICES UNIT, 1994). Their results indicated that in the near-shore zone, storm surges ranging from 4–7 m would be increased by a further 0.3–0.7 m due to wave set-up.

Figures 6A and B show the modelled sea levels at Port Hedland harbour and Port Hedland hotel, respectively. The peak sea levels inside Port Hedland hotel reached 5.7 m above mean sea level, while the model produced a peak of 5.3 m. Since the observed sea level peak contains a contribution from wave set-up of between 0.4 to 0.6 m, the model simulation of the storm surge and tide indicates remarkably close agreement with observations.

Figure 7 shows the inundation at three stages during the cyclone event. While detailed verification of the model results is not possible, comparison with aerial photographs taken on the west side of Port Hedland township after the floods and showing the maximum water level attained during the surge, indicate good qualitative agreement. Flooding in the township is reported to have developed from the south initially with the water flowing in from the east. Modelled results shown in Figure 7a match these anecdotal reports. It is later reported to have flowed in from the west once the seawall was breached and finally in over the higher ground to the north. Figure 7b shows the simulated flooding occurring in these locations. After the peak, the water apparently drained into the swamp to the south of the town. Model simulations shown in Figure 7c also indicate draining of water to the south of the town.

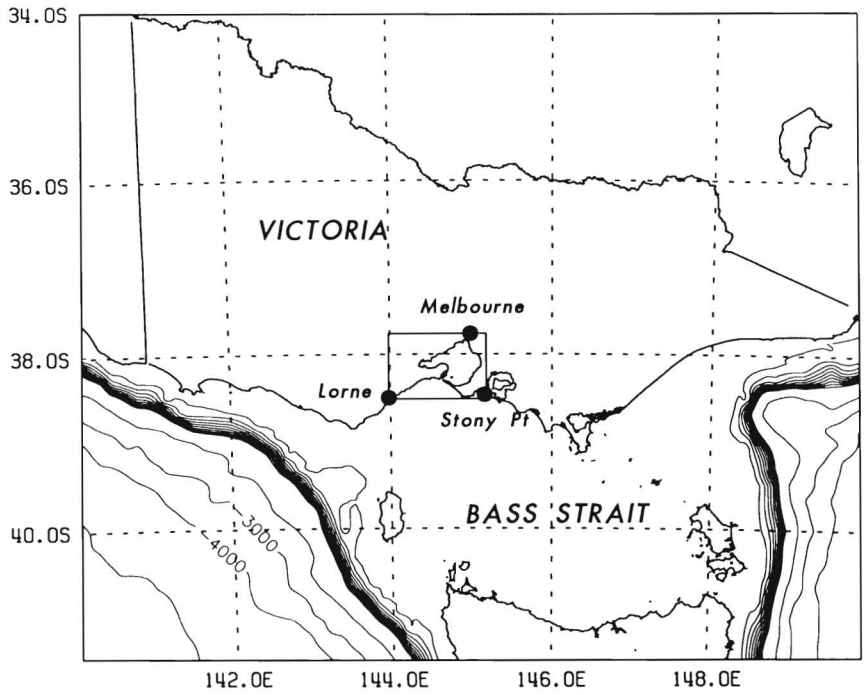

Figure 8. Map showing the location of Port Phillip Bay (inside inner rectangular region) and surrounding locations. Bathymetric contours are at 100 m intervals up to 1000 m and 1000 m intervals thereafter.

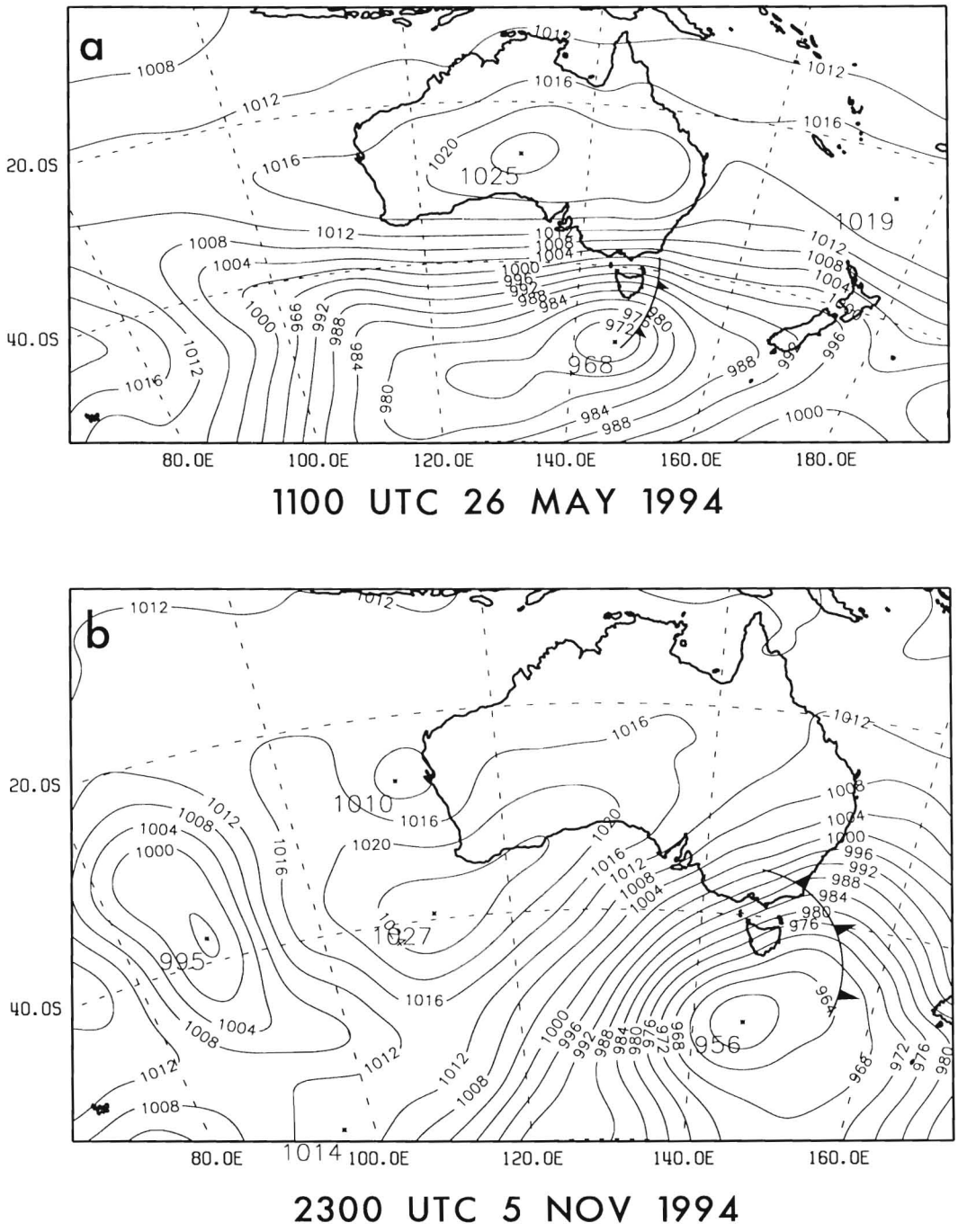

Figure 9. Mean sea level pressure analyses at the closest available time to when the peak storm surge was experienced in Port Phillip Bay for (a) the May event and (b) the November event.

Comparison of Fixed and Moving Coastline Boundary Conditions

In this section, the differences in coastal storm surge heights which result from the two different treatments of the coastal boundary are examined. Six coastal locations marked w1, w2, e1, e2, e3 and e4 have been selected and are indicated in Figure 5. Modelled sea level heights at each of these locations from west to east are 5.3, 5.1, 5.3, 5.2, 5.4 and 5.7 m respectively. In comparison, the fixed-coastline boundary condition leads to storm surge peaks at these locations of 5.4, 5.4, 5.6, 5.4, 6.3 and 5.8 m which range from between 2 and 17% higher. The largest differences occur at coastal points

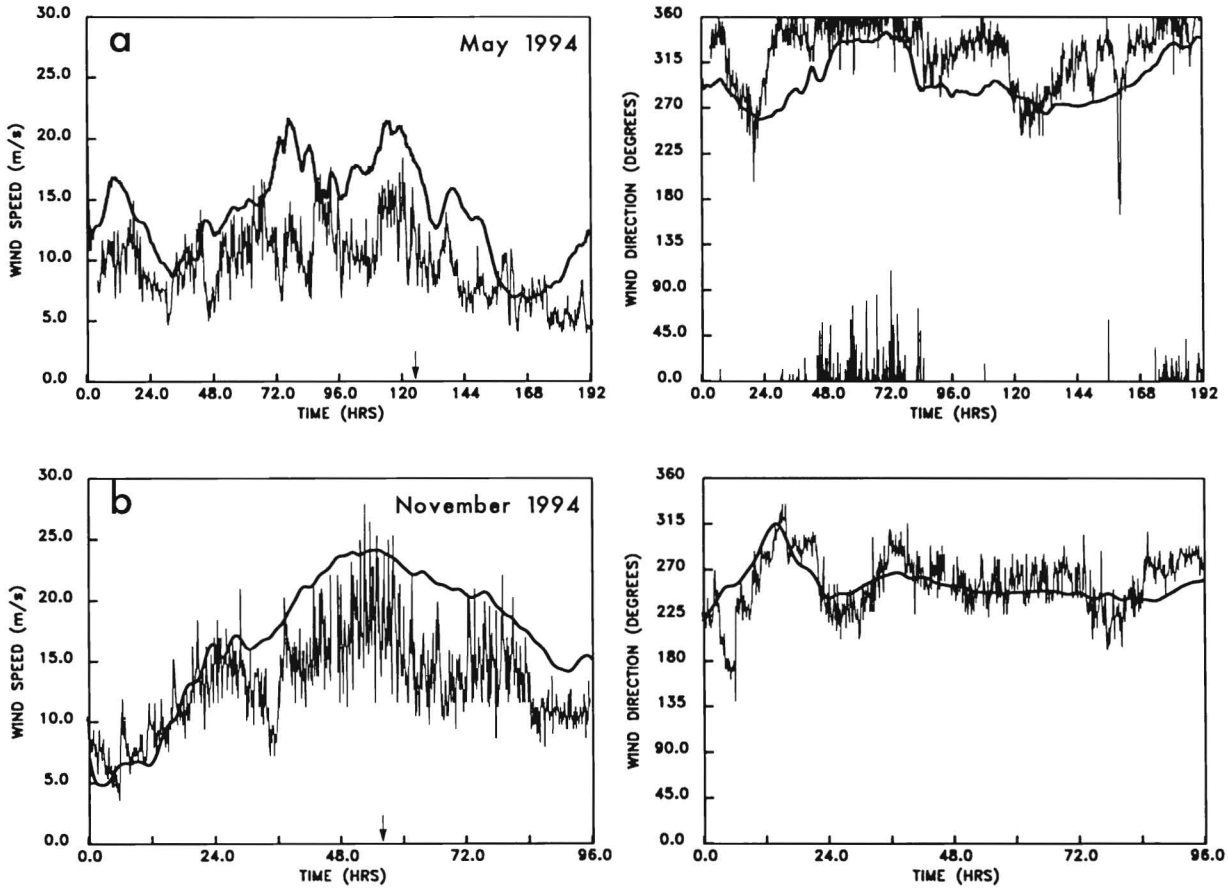

Figure 10. Modelled and observed wind speed (left) and direction (right) for (a) the May cold front event commencing at 1100 UTC 21 May 1994 and (b) the November event commencing at 2300 UTC 3 November 1994. The arrows on each of the horizontal axes of the wind speed diagrams mark the time of peak storm surge at St Kilda.

which are located in embayments, particularly when backed by low-lying coastal terrain. The tendency for fixed-coast models to overestimate storm surge heights has also been shown by YEH and CHOU (1979).

Sensitivity of Results to Grid Resolution

The robustness of the scheme developed in the present study is demonstrated in this section by comparing results obtained using lower grid resolution. FALCONER and OWENS (1987) have reported that in their experience, inundation algorithms which rely on instantaneous wetting and drying of grid cells can become numerically unstable when the model resolution is reduced. Ideally, an inundation scheme should not only remain stable but should produce fairly consistent results despite variations in grid resolution. It is noteworthy that in an earlier version of the present model, in which the wetting and drying criterion was of the type described in Falconer and Owens, the model tended to become numerically unstable when grid resolution was reduced.

Three experiments with grid resolutions of 150, 225, and 300 m, respectively, were conducted to test model sensitivity to changes in grid spacing. Results of these tests are given in Table 1. The number of inundated grid cells and corresponding area have been calculated for the time of peak surge and three hours before and after the peak. The standard deviations do not exceed 10% and tend to be slightly lower during the draining phase, possibly because draining is occurring at a slower rate than flooding. The 150 and 300 m resolutions produce values that are in closer agreement than the 225 resolution simulation. This result reflects the greater difference in topographical representation between the 150 m and the 225 m since the latter required interpolation whereas the 300 m grid simply utilized every second gridpoint of the 150 m grid.

STORM SURGE INUNDATION MODELLING IN PORT PHILLIP BAY

Background

Storm surges in Port Phillip Bay are most frequently caused by periods of sustained westerly winds which occur when cold fronts travel along the southern Australian coast (MCINNES and HUBBERT, 1996). The two events modelled in the present study occurred in May and November 1994. An

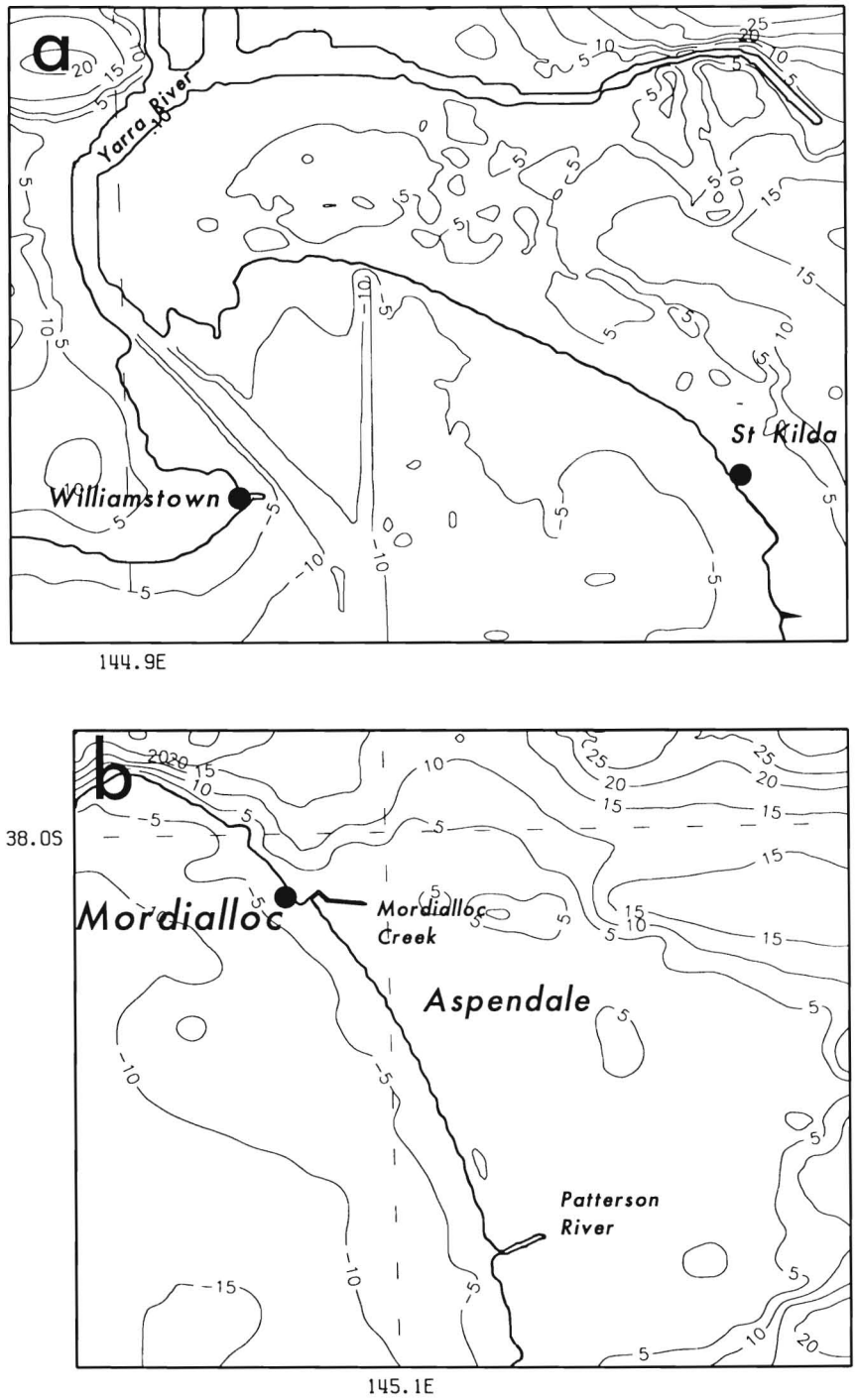

Figure 11. (a) The Hobsons Bay fine mesh model domain and (b) the Mordialloc model domain. Topography and bathymetry contours are shown at 5 m intervals and relevant features are labelled.

examination of the residual sea level signals (total sea level minus tide) at Lorne and Stony Point in Bass Strait, and Williamstown at the northern end of the bay (see Figure 8 for locations) indicate that sea levels within the Bay are closely related to those occurring on the open coastline, although some attenuation of the signal generally occurs at Williamstown.

The observed maximum sea level heights at Williamstown

Table 2. *Summary of the simulated peak sea level heights for the May and November storm surge events at Werribee (W), St Kilda (SK) and Mordialloc (M). See Figure 11 for locations.*

Experiment No	Description	Hobsons Bay		Mordialloc	
		May	November	May	November
1	Control	0.9	0.9	0.5	0.5
2	80 cm sea level rise	1.7	1.8	1.4	1.6
3	80 cm slr + 10% increase in winds	2.3	2.9	2.7	1.7
4	As for 2 but no levees			6.5	6.2
5	As for 3 but no levees			7.5	8.8

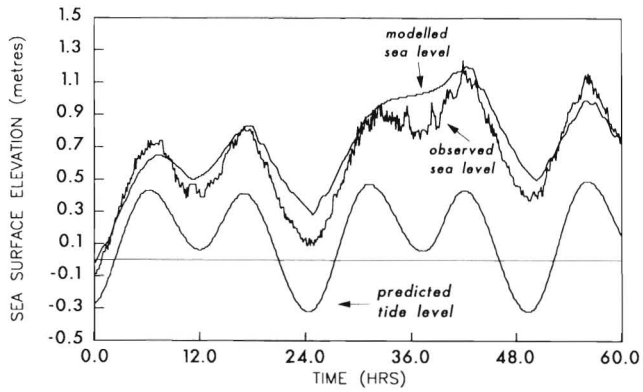

Figure 12. Curves showing the observed and modelled sea levels at St Kilda over a 60 hour interval commencing at 2300 UTC 24 May 1994. The predicted tide at Williamstown is also shown. All sea levels are referenced to AHD.

for the May and November cases were 1.046 and 1.074 m above the Australian Height Datum (AHD)† respectively. Based on the return period analysis of ADAMS (1987), these events have return periods at Williamstown of between two and five years.

Meteorology and Atmospheric Boundary Conditions

The sea level pressure pattern at the time closest to the peak surge in Port Phillip Bay for each of the events is shown in Figure 9. The May event commenced with a cold front located at the southwestern tip of Western Australia at 0000 UTC 23 May 1994. During the next four days, it travelled eastward along the south coast of the continent producing elevated westerly winds and sea levels at tide gauges all the way along the south coast.

The strong winds and elevated sea levels of the November event were confined to the western half of the southern coastline due to the presence of a ridge of high pressure located over the south west corner of the continent. Winds accompanying this front were from a slightly more south-westerly direction compared with the May case.

Rainfall was not extreme for either the May or November events with maximum 24 hour totals recorded at Melbourne

† AHD is approximately equal to mean sea level.

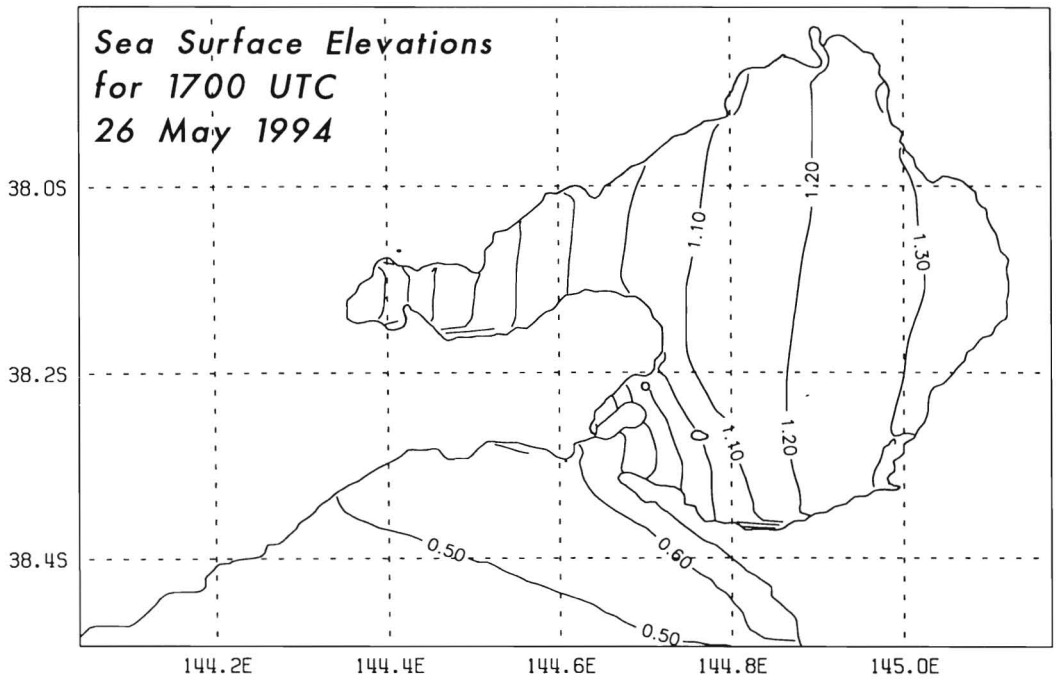

Figure 13. Model simulated sea surface elevations for 1700 UTC 26 May 1994. Units are in m and sea levels are referenced to AHD.

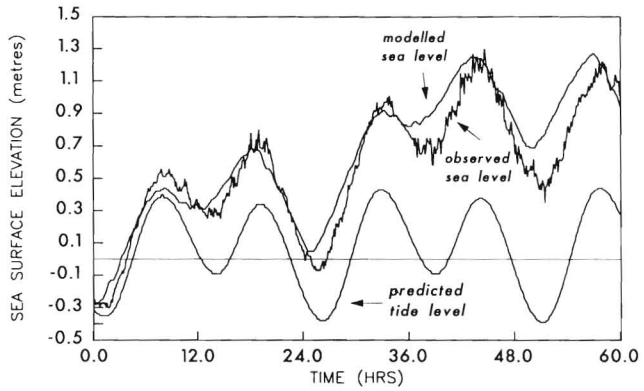

Figure 14. Curves showing the observed and modelled sea levels at St Kilda over a 60 hour interval commencing at 1100 UTC 4 November 1994. The predicted tide at Williamstown is also shown. All sea levels are referenced to AHD.

not exceeding 3 mm and 5 mm respectively for the duration of the events. However, due to the high sea levels which backed up through the storm water drains in some low lying bayside suburbs of Melbourne, accumulated rainfall was reported to have caused minor flooding in some areas.

Atmospheric surface pressure and winds for the various storm surge model simulations were obtained by running an atmospheric model based on McInnes and Hess (1992) at 25 km horizontal resolution over the region bounded by 27°S, 45°S, 125°E and 153°E. Fifteen vertical levels were used with the lowest model level located at approximately 10 m above the surface. Initial and boundary conditions for the atmospheric model were obtained by interpolating 12 hourly Australian Bureau of Meteorology analyses (Mills and Seaman, 1990), to the atmospheric model grid. The simulation for the May event was conducted over an eight day interval from 1100 UTC 21 May 1994. For the November event, the model was run over a four day interval from 2300 UTC 3 November 1994. A comparison of the modelled and observed winds at St Kilda for both simulations are shown in Figure 10 and indicate that the model has represented the timing of the wind changes reasonably well although the wind speed has been slightly overestimated. Surface pressure and 10 m winds from the atmospheric model were stored every six hours and spatially interpolated to the appropriate storm surge model domain to provide surface boundary conditions for the storm surge model.

Model Methodology

Storm surge model simulations were carried out on a 500 m resolution Port Phillip Bay domain indicated in Figure 8. Both the May and November events were run out for 60 hours commencing at 2300 UTC 24 May 1994 and 1100 UTC 4 November 1994, respectively. The sea level heights at the open boundary of the storm surge model in Bass Strait were obtained by linearly interpolating observed sea levels at Lorne and Stony Point.

The storm surge model was then run over the two smaller regions shown in Figure 11. The grid resolutions on the Hobsons Bay and Mordialloc regions were 30 m and 50 m re-

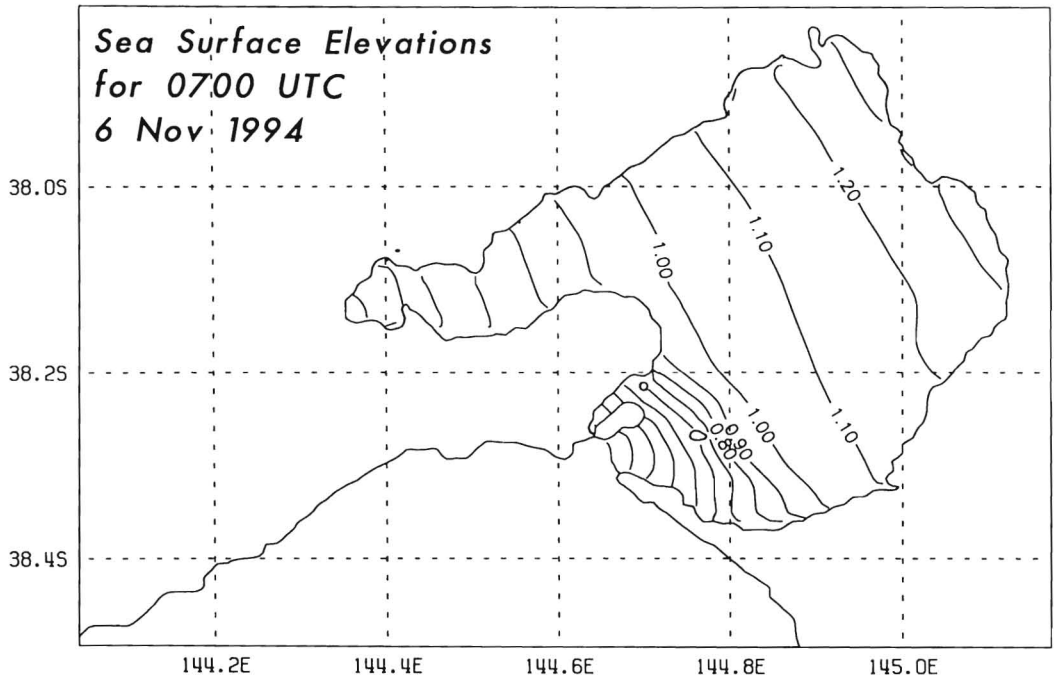

Figure 15. Model simulated sea surface elevations for 0700 UTC 6 November 1994. Units are in m and sea levels are referenced to AHD.

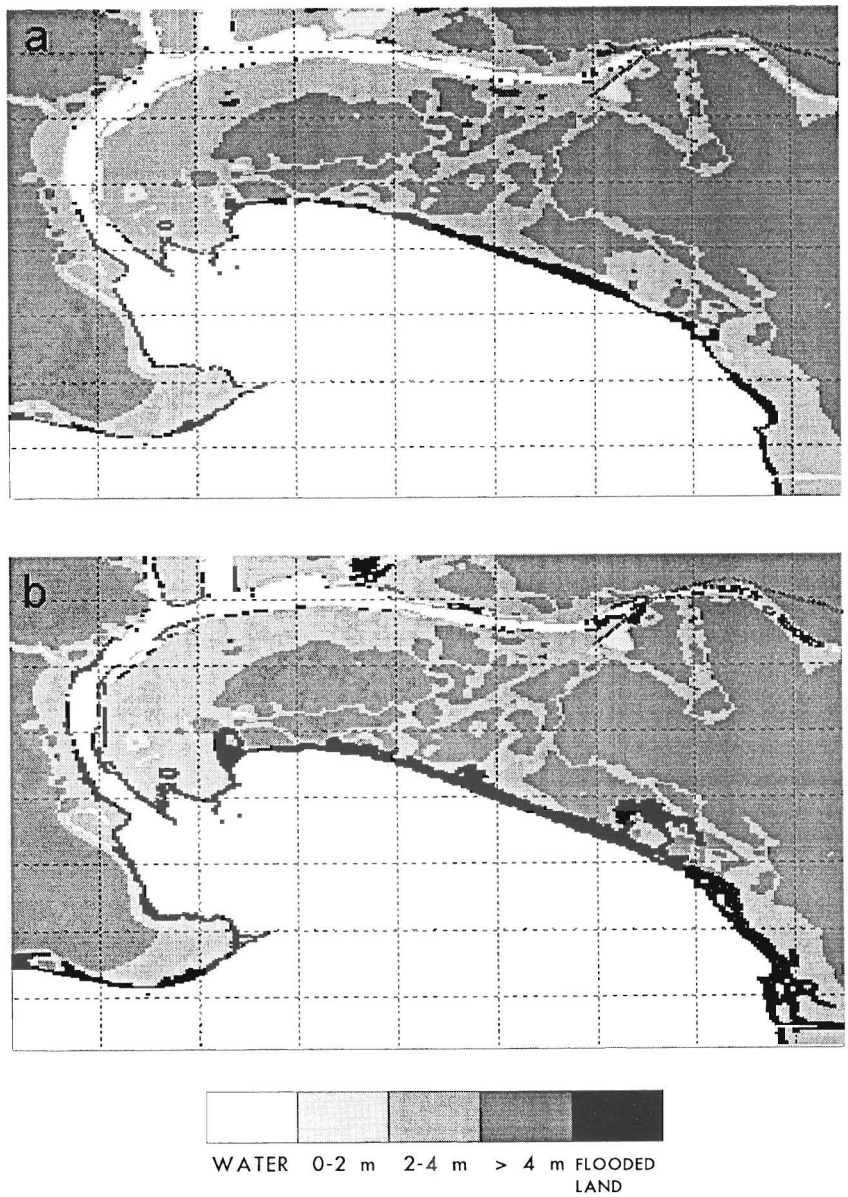

Figure 16. The peak storm surge inundation on the Hobsons Bay domain for (a) the control experiment and (b) experiment 3. Gridlines indicate a spacing of 1 km.

spectively. Bathymetric data for these regions was manually digitized from shipping charts. High resolution digital representation of the 0, 1.0, 2.0 and 3.0 m contours were interpolated to the model grids. Tributaries were included and flow rate data used to input the appropriate mass flux at these locations. On the Mordialloc domain, the width of the tributaries in the model was increased to about four model gridpoints to ensure numerical stability.

Sensitivity Experiments

A series of sensitivity experiments were performed over the outer and two inner regions for each of the storm surge events and these are described in Table 2. The purpose of the simulations was to investigate the vulnerability of the two inner regions to sea level rise and varied storm strength as well as highlight the importance of maintaining and possibly increasing the height of the levee banks on the Mordialloc Creek in view of the potential impact of climate change. Experiment 1 is the control experiment used to benchmark the subsequent experiments.

In experiment 2, the mean sea level was increased by 0.8 m. This value corresponds to a worst-case scenario of possible sea level rise due to the enhanced greenhouse effect which would be expected to occur when atmospheric CO_2 levels

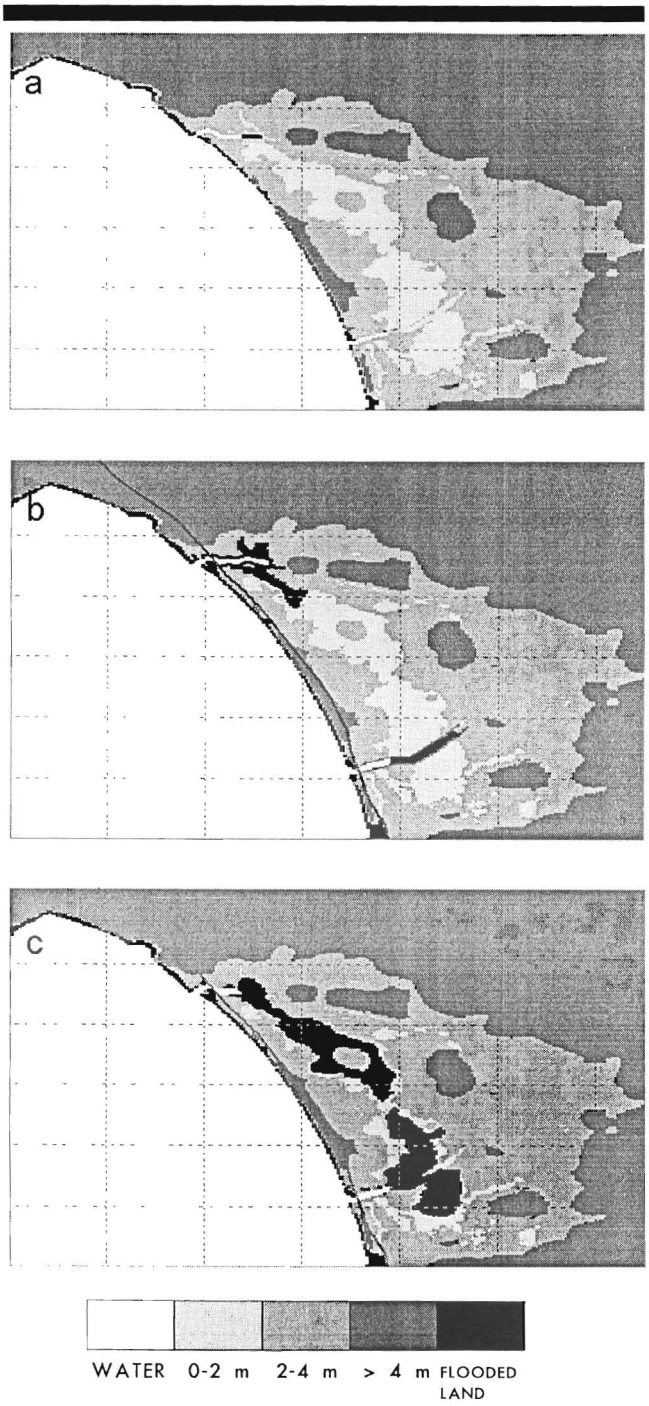

Figure 17. The peak storm surge inundation on the Mordialloc domain for (a) the control experiment, (b) experiment 3 and (c) experiment 5. Gridlines indicate a spacing of 2 km.

reach twice their pre-industrial values (in about 2070) (WHETTON *et al.*, 1995). It should be noted however, that since the worst case scenario has been used, it is unlikely that such extreme sea level rise would be experienced by this time (MCINNES and HUBBERT, 1996; WHETTON *et al.*, 1995).

In experiment 3, the impact of a stronger storm is simulated by taking the existing situations and increasing the wind strength uniformly by 10%. For consistency, boundary conditions at the open boundary required altering for this experiment also. The surges in Port Phillip Bay are highly correlated with those which occur on the open coastline as previously discussed. MCINNES and HUBBERT (1996) show that a 10% increase in wind strength for these two storms on the open coastline produces approximately a 20% increase in storm surge height at the coast. This response is related to the wind stress terms $\tau_s/\rho_a H$ in (1) and (2) where τ_s is a function of the wind speed squared as well as the drag coefficient, C_D, which itself is a function of the wind speed. Therefore, on the open boundary, the residual component of the sea level height was increased by 20%. For this experiment, the 80 cm sea level rise was also imposed.

Experiments 4 and 5 involved only the Mordialloc domain under conditions of increased sea level and storm strength and involved running the model in the absence of the existing levee banks on the Mordialloc Creek to demonstrate their importance under these conditions. In all experiments, the inflow rates of the various river systems were held constant.

Table 3. *Summary of the area inundated over Hobsons Bay and Mordialloc for the various experiments. Units are km².*

	May 1994			November 1994		
	W	SK	M	W	SK	M
EXP 1	0.92	1.20	1.30	0.94	1.25	1.28
EXP 2	1.72	2.01	2.11	1.75	2.06	2.08
EXP 3	1.95	2.22	2.35	1.97	2.31	2.35

Storm Surge and Inundation Results

The results on the outer domain encompassing Port Phillip Bay are presented and discussed first. Time series of modelled and observed sea level height at St Kilda are compared in Figure 12 for the May event. Both time series show reasonably close agreement, although the modelled height tends to be slightly over-predicted, particularly at low tide. This error is most likely due to the slight overestimation of the wind speed by the atmospheric model. Because of the orientation of the entrance into Port Phillip Bay, ebb tide currents through this channel will tend to be slowed by the prevailing westerlies, leading to relatively higher water levels at low tide. The predicted tide level is shown also and indicates that observed sea levels for this event were up to 0.8 m higher than normal. The spatial variation of the surge across the bay is shown in Figure 13 at the time of the peak surge at St Kilda. A pronounced east-west gradient is evident with the highest surge located on the eastern side of the bay. This is caused by wind set-up, produced by the westerly winds within Port Phillip Bay. The modelled peak sea levels for this event at St Kilda, Werribee and Mordialloc are summarised in Table 3 and reflect this gradient with the peak surge height at Mordialloc being 0.38 m higher than at Werribee.

In Figure 14, the modelled and observed time series at St Kilda for the November case are shown. The modelled storm surge heights show close agreement with observations at

high tide, although again water levels are over-estimated at low tide. This storm produced a slightly higher storm surge at St Kilda than the May event. The predicted tide levels indicate that about 0.9 m of the maximum sea level was due to the storm surge. At Mordialloc, the peak surge for November is slightly lower than the May case. This difference is due to a slightly more southerly component in the winds during the November event which produced sea level height contours that were aligned with more of a northwest-southeast orientation (Figure 15).

Inundation results for the control simulation over Hobsons Bay and Mordialloc are shown for the November case in Figures 16a and 17a respectively. In both locations, the inundation is confined to the beach front. This result is consistent with the extent of inundation observed during both events. Converting the inundated grid cells into an aerial coverage yields a total area inundated of 0.9 km^2 over Hobsons Bay and 0.7 km^2 over Mordialloc.

Application to Climate Change Scenarios

Results from the sensitivity experiments are now discussed. Areas of inundation for all sensitivity experiments are summarized in Table 2 while sea level height for experiments 2 and 3 are summarized in Table 3.

In experiment 2, maximum sea level heights at each location are approximately 0.80 m higher than the control experiment for both cases. The additional increase in background winds in experiment 3 produces a further increase in sea level heights of between 0.21–0.27 m, with relatively higher sea levels occurring on the eastern side of the bay.

Over Hobsons Bay, experiment 2 produces a doubling of the area inundated in both the May and November storm events. Over Mordialloc, there is approximately a threefold increase in the area of inundation with some breaching of the levee banks on the north and south sides of the Mordialloc Creek (not shown).

The 10% increase in winds combined with the sea level rise in experiment 3 further increases the area inundated over the Hobsons Bay region to 2.3 and 2.9 km^2 for the May and November cases respectively indicating that this region is more sensitive to the west-southwesterly oriented winds of the November case than the westerly winds of the May case. As indicated in Figure 16B for the November case, some inundation is occurring in low lying residential areas. Over the Mordialloc region however, the greatest increase in inundation accompanies the more westerly winds of the May case (2.7 km^2) compared with 1.7 km^2 for the November case. The area under water is located slightly further eastward than experiment 2, consistent with the stronger westerly winds (Figure 17b).

Experiments 4 and 5 were conducted to demonstrate the important role played by the existing levee banks on both rivers in the Mordialloc domain by removing them in the model simulations. As expected, the results show greatly increased flooding under conditions of sea level rise and increased wind strength. The results of experiment 5 for the November case are shown in Figure 17c.

The sensitivity experiments serve to illustrate several points. Firstly, while many coastal regions may be well protected from the effects of severe weather events under present climate conditions, this may not be the case if the mean climatic state changes. It is worth reiterating that the scenario for mean sea level rise used in the present study is at the extreme end of the range of possibility for 2070 and there is no evidence at this stage to suggest that westerly wind events would on average increase in intensity under enhanced greenhouse conditions; a decrease of the same magnitude being equally possible (McInnes and Hubbert, 1996). However, it should also be noted that the two storm surges modelled in the present study are not particularly rare events, and a more intense storm surge could produce just as much inundation under a lower rise in sea level. Furthermore, storm surges which coincide with heavy rainfall events could produce greater inundation due to the combined effects of increased river flow rates and elevated sea levels in the bay. Neither of the surge events modelled in the present study were associated with high rainfall, although such events have occurred in this region over the last century (McInnes and Hubbert (1996) and Adams (1987)).

CONCLUSIONS

A storm surge model with inundation capabilities has been developed for application to coastal planning and storm impact studies. The model is designed to be easily re-locatable to other geographical regions and multiple nesting of model simulations enables the more accurate specification of boundary conditions on the high resolution inner model grids. The coastal boundary of the model is moveable and a wetting and draining technique, with constraints on the sea level height and current speed, is applied to determine when gridpoints are added to or removed from the computational domain.

The model's capabilities for predicting inundation and storm surge are demonstrated by its application to two distinct geographical regions under markedly different meteorological forcing. In the first instance, severe inundation produced by an intense tropical cyclone on the open coastline of northwest Australia is modelled and shown to produce realistic results when compared with available observations. In the second instance, the model is successfully applied to two regions within an enclosed bay in the southwest of the continent under atmospheric forcing produced by two severe wintertime cold fronts.

Comparisons made between the storm surge heights produced using fixed coastline and moving coastline boundary conditions, indicated that the maximum heights at the coast are greater by up to 17% when fixed coastline boundary conditions were used. This result has serious implications for studies where flood levels from storm surges are determined from fixed coastline storm surge model results.

Simulations conducted with reduced model resolution showed, not only that the model remains stable when run over the region with fewer gridpoints, but that there is a high level of agreement between simulations on the total area inundated. This result is attributed to the use of the flow rate in the inundation algorithm which prevents instantaneous wetting and drying of grid cells simply because the water

depth criterion has been satisfied. When flow rates are not taken into consideration, degraded grid resolution can increase rates of inundation leading to at best, unrealistic flood rates and at worst, numerical instability.

Scenarios of sea level rise and increased storm wind strength were imposed on the model simulations to explore the possible impact of climate change on two potentially vulnerable regions in southeastern Australia as well as demonstrate the application of the model to impact studies of this kind. Results highlighted the site and storm specific nature of coastal flooding. Levee banks on one of the tributaries in the model domain were found to be inadequate under the extreme scenarios imposed and suggested that this region could also be vulnerable to a more extreme storm even without a large rise in mean sea level.

ACKNOWLEDGMENTS

The first author wishes to acknowledge the work of Stuart Smith in researching much of the historical data surrounding the Port Hedland tropical cyclone event. In addition, he would also like to thank Bob Cunning and Ralph Ninham of Cargill Salt Ltd.; Dick Reeson of Saltech, Warren Jacka of Roebourne Surveying and Mapping; Barry Hanstrum, Joan Trevers, Gary McCall, Chris Blackford and Ray Stockdom of the Bureau of Meteorology, Australia and Rick Mahoney of Coastal Information and Engineering Services. He is also grateful to the assistance provide by Aerial Associated Mapping Surveys and BHP Iron Ore.

Both authors are grateful to a number of people who assisted with aspects of the Port Phillip Bay study. These people include, Paul Doherty (MITS), Dennis Hearn (EPA), and Peter Newton and Gerardo Trinidad (CSIRO Division of Building Construction and Engineering), Geoff Crapper, Martin Dunkley and Keith Bonaface (Melbourne Water), and Robert Molloy of the CSIRO project team of the Port Phillip Bay study who assisted in the provision of topographic and bathymetric data for the high resolution grids within Port Phillip Bay. Sea level data for verification of the storm surge models were obtained from various sources. The authors wish to thank Bill Mitchell and Marion Tate from the National Tidal Facility for providing the sea level data at Lorne, Stony Point and Williamstown. Geoff Crapper provided storm surge and wind verification data for St Kilda, as well as river flow rate information. Finally, the authors wish to thank Peter Whetton, Anthony Hirst and Barrie Pittock for valuable comments on the manuscript. Part of this study was funded by the Victorian EPA and Melbourne Water.

LITERATURE CITED

ADAMS, J. R., 1987. Tide levels during November–December 1934. Flood and high tide frequency analysis for Williamstown, Board of Works Internal Report, 64p.

FALCONER, R. A. and OWENS, P. H., 1987. Numerical simulation of flooding and drying in a depth-averaged tidal flow model. *Proceedings Institution Civil Engineers*, 83, 161–180.

FLATHER, R. A., 1994. A storm surge prediction model for the northern Bay of Bengal with application to the cyclone disaster in April 1991. *Journal Physical Oceanography*, 24, 172–190.

FLATHER, R. A. and HEAPS, N. S., 1975. Tidal computations for Morecambe Bay. *Geophys. Journal Royal Astronomical Society*, 42, 489.

FLATHER, R. A. and HUBBERT, K. P., 1990. Tide and surge models for shallow water-Morecambe Bay revisited. *In:* A. M. DAVIES *Modelling Marine Systems*, Boca Raton Florida, CRC Press, vol 1, pp. 135–166.

FLATHER, R. A. and KHANDKER, H., 1993. The storm surge problem and possible effects of sea level changes on coastal flooding in the Bay of Bengal. *In:* R. A. WARRICK; E. M. BARROW and T. M. WIGLEY (eds.). *Climate and Sea Level Change; Observations, Projections and Implications*, Cambridge University Press, 229–245.

FLATHER, R. A.; PROCTOR, R. and WOLF, J., 1991. Oceanographic forecast models. *In:* D. J. FARMER and M. J. RYCROFT. *Computer Modelling in the Environmental Sciences*, Oxford: Clarendon Press, pp. 15–30.

HOLLAND, G. J., 1980. An analytical model of wind and pressure profiles in hurricanes. *Monthly Weather Review*, 108, 1212–1218.

HUBBERT, G. D.; HOLLAND. G. J.; LESLIE, L. M., and MANTON, M. J., 1991. A real-time system for forecasting tropical cyclone storm surges. *Weather and Forecasting*, 6, 86–97.

HUBBERT, G. D.; LESLIE, L. M. and MANTON, M. J., 1990. A storm surge model for the Australian region. *Quarterly Journal Royal Meteorological Society*, 116, 1005–1020.

JARVINEN, B. R. and LAWRENCE, M. B., 1985. An evaluation of the SLOSH storm-surge model. *Bulletin American Meteorological Society*, 66, 1408–1411.

KONISHI, T., 1995. An experimental storm surge prediction for the western part of the Inland Sea with application to Typhoon 9119. *Papers in Meteorology and Geophysics*, 46, 9–17.

LEENDERSTE, J. J. and GRITTON, E. C., 1971. *A Water Quarterly Simulation Model for Well Mixed Estuaries and Coastal Seas, Vol. II, Computation procedures*. New York: The Rand Corporation.

MCINNES, K. L. and HESS, G. D., 1992. Modifications to the Australian region limited area model and their impact on an east coast low event. *Australia Meteorological Magazine* 40, 21–31.

MCINNES, K. L. and HUBBERT, G. D., 1996. *Extreme Events and the impact of Climate Change on Victoria's Coastline,* Environment Protection Authority, State Government of Victoria, Publication 488, 69pp.

MESINGER, F. and ARAKAWA, A., 1976. *Numerical Methods Used in Atmospheric Models*. GARP Publ. Ser. No. 17, ICSU/WMO.

MILLER, M. J. and PEARCE, R. P., 1974. Numerical model of a cumulonimbus. *Quarterly Journal Royal Meteorological Society*, 100, 133–154.

MILLER, M. J. and THORPE, A. J., 1981. Radiation conditions for the lateral boundaries of limited-area numerical models. *Quarterly Journal Royal Meteorological Society*, 107, 615–628.

MILLS, G. A. and SEAMAN, R. S., 1990. The BMRC Regional Data Assimilation System. *Monthly Weather Review*, 118, 1217–1237.

REID, R. O. and BODINE, B. R., 1968: Numerical model for storm surges in Galveston Bay. *Journal Waterways and Harbors Division*, 9, 35–57.

SIELECKI, A. and WURTELE, M. G., 1970. The numerical integration of the nonlinear shallow-water equations with sloping boundaries. *Journal Computational Physics*, 6, 219–236.

SIGNELL, R. P. and BUTMAN, B., 1992. Modeling tidal exchange and dispersion in Boston Harbor. *Journal Geophysical Research*, 97, 15591–15606.

SMITH, S. D. and BANKE, E. G., 1975. Variation of the sea surface drag coefficient with wind speed. *Quarterly Journal Royal Meteorological Society*, 101, 665–673.

SPECIAL SERVICES UNIT, 1994. *Port Hedland Salt Works Storm Surge Inundation Study*. Report No. SSU94-2, prepared by Special Services Unit, Bureau of Meteorology, Melbourne.

WHETTON, P. H.; MULLAN, A. B. and PITTOCK, A. B., 1995. Climate Change Scenarios for Australia and New Zealand. *In:* PEARMAN, G. I. and MANNING, M. (eds.), *Proc. Greenhouse 94*, (Wellington, 9–14 October 1994), CSIRO Publishing, pp. 145–168.

YEH, G.-T. and CHOU, F.-K., 1979. Moving boundary numerical surge model. *Journal Waterways Port Coastal and Ocean Division*, 105, 247–263.